

Jet substructure measurements with ALICE

R. Vártesi^{a,1} (for the ALICE Collaboration)

^aWigner Research Centre for Physics, MTA Centre of Excellence,
29-33 Konkoly-Thege Miklós út, 1121 Budapest, Hungary

A selection of new jet substructure measurements are reported from the ALICE experiment at the CERN LHC in both proton-proton and heavy-ion collisions. These include the first fully corrected inclusive measurements of the groomed jet momentum fraction and the groomed jet radius, as well as the N -subjettiness distribution and the fragmentation distribution of reclustered subjets. We also report on the measurement of several groomed substructure observables of heavy-flavor jets in pp collisions, fragmentation functions and the new measurements of the radial distributions of D^0 mesons or Λ_c^+ baryons in jets. The measurements are compared to theoretical calculations and provide new constraints on the physics underlying parton fragmentation and jet quenching.

PACS: 25.75.-q; 12.38.Mh; 95.30.Cq; 13.85.-t

1. Introduction

Jet substructure measurements, based on the distribution of constituents within a jet, are able to probe specific regions of QCD radiation phase space for jet showers in vacuum. This powerful capability provides new opportunities to study fragmentation patterns of parton showers in vacuum and the dynamics of jet quenching in heavy-ion collisions.

The ALICE detector [1] has unique capabilities for jet substructure measurements, due to its high-precision tracking system and focus on jets with low transverse momenta. Charged-particle jets are clusterized using the anti- k_T algorithm [2] from tracks that are reconstructed in the Inner Tracking System and the Time Projection Chamber, with a high spatial precision in the full azimuth angle φ and the pseudorapidity range $|\eta| < 0.9$. Full jets reconstructed using the Electromagnetic Calorimeter in a more limited acceptance ($1.4 < \varphi < \pi$, $|\eta| < 0.7$) allow for a more direct access to parton kinematics.

Heavy-flavor hadrons are identified from their decay products, utilizing tagging algorithms based on the displacement of the secondary decay vertex. The excellent tracking capabilities of the ALICE detector allow for jet substructure studies for heavy-flavor as well as untagged jets. Heavy-flavour jets are declustered to trace all branchings of the charm quark and to reveal mass dependence of the shape and structure of the parton shower due to the dead-cone effect [3].

In the following sections, a selection of recent ALICE results is presented on inclusive untagged-jet and charm-jet substructure observables in proton-proton collisions, followed by results on jet substructure in heavy-ion collisions.

¹E-mail: vertesi.robort@wigner.hu

2. Groomed jet substructure of inclusive jets in pp collisions

Jet grooming algorithms are used to access the hard parton structure of a jet. By mitigating the influence from the underlying event and hadronization processes, perturbative quantum chromodynamics (pQCD) calculations can be directly compared to groomed-jet observables. A popular novel technique, soft-drop (SD) grooming [4], aims for the removal of large-angle soft radiation. In this method, the jets that had previously been reconstructed with the anti- k_T algorithm [2] are reclustered using the Cambridge-Aachen (C/A) algorithm [5] to form a clustering tree that follows angular ordering. Then the soft branches are iteratively removed if not fulfilling the so-called soft-drop condition,

$$z > z_{\text{cut}} \theta^\beta, \quad \text{where} \quad z = \frac{p_{T,2}}{p_{T,1} + p_{T,2}} \quad \text{and} \quad \theta = \frac{\Delta R_{1,2}}{R} \quad (1)$$

are the momentum fraction taken by the subleading prong ($p_{T,1}$ and $p_{T,2}$ being the momenta of the two prongs), and the splitting radius (defined as the ratio of the $\Delta R_{1,2}$ splitting angle between the two prongs and the resolution parameter R of the anti- k_T clustering). The soft threshold z_{cut} determines the overall strength of the grooming, and the angular exponent β controls the strength with which wide-angle soft radiation is rejected. The groomed-jet substructure is often characterized by the groomed momentum fraction z_g and the groomed radius θ_g , defined as the values of z and θ corresponding to the first hard splitting fulfilling the soft-drop condition. In addition, the number of groomed-jet splittings fulfilling the SD-condition along the hardest branch, n_{SD} , is also used to quantify the jet substructures. ALICE measurements of charged-particle-jet θ_g , z_g and n_{SD} in pp collisions are well-described by model calculations [6, 7].

Jet structure can also be characterized with the generalized jet angularities

$$\lambda_\alpha^\kappa = \sum_i z_i^\kappa \theta_i^\alpha, \quad \text{where} \quad z_i = \frac{p_{T,i}}{p_{\text{T}}^{\text{jet}}} \quad \text{and} \quad \theta_i = \frac{\Delta R_i}{R} \quad (2)$$

are the momentum fraction and angular deflection of the i^{th} constituent within the jet [8]. The generalized jet angularities are infrared- and collinear-safe quantities in case of $\kappa = 1$ and $\alpha > 0$, in which case they can be directly calculated from pQCD. The special cases λ_1^1 and λ_2^1 reduce to the jet girth and jet thrust. With the comparison of λ_α^κ for groomed and non-groomed jets, with the systematic variation of α , the interplay between the perturbative and non-perturbative regimes of the QCD can be explored in detail, and strong constraints can be established for pQCD and fragmentation models.

Figure 1 shows the generalized jet angularities measured by the ALICE experiment in pp collisions at $\sqrt{s} = 5.02$ TeV for different α values for ungroomed (top) and SD-groomed jets (bottom) [9]. The data are also compared to next-to-leading-logarithmic (NLL') calculations [10] with

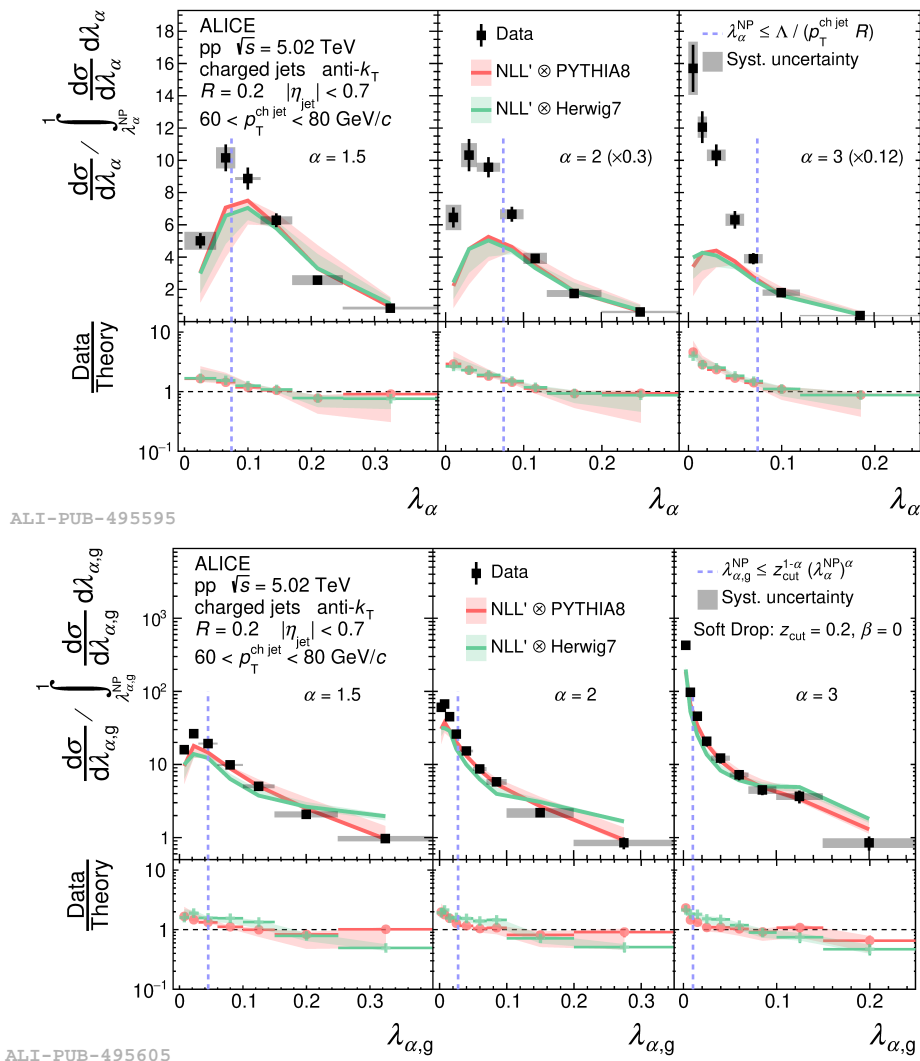


Fig. 1. Comparison of ungroomed (top) and groomed (bottom) charged-particle jet angularities in pp collisions for $R = 0.2$ to analytical NLL' predictions with MC hadronization corrections in the range $60 < p_{T,\text{ch,jet}} < 80$ GeV/c [9]. The dashed blue line indicates the boundary between the non-perturbative and perturbative regimes.

PYTHIA8 [11] as well as Herwig7 [12] fragmentation. In the ungroomed case, a significant deviation can be observed in the non-perturbative regime, toward smaller λ_α values. The deviation is more pronounced in the case the α exponent is larger. As expected, the data is better reproduced by the models in the groomed case, as the perturbative regime is significantly extended by SD grooming.

3. Flavor dependence of the jet structure

Due to their large mass, heavy-flavor hadrons are produced in perturbative processes down to low transverse momenta. Since heavy-flavor quarks undergo weak decay, their numbers remain largely unchanged throughout

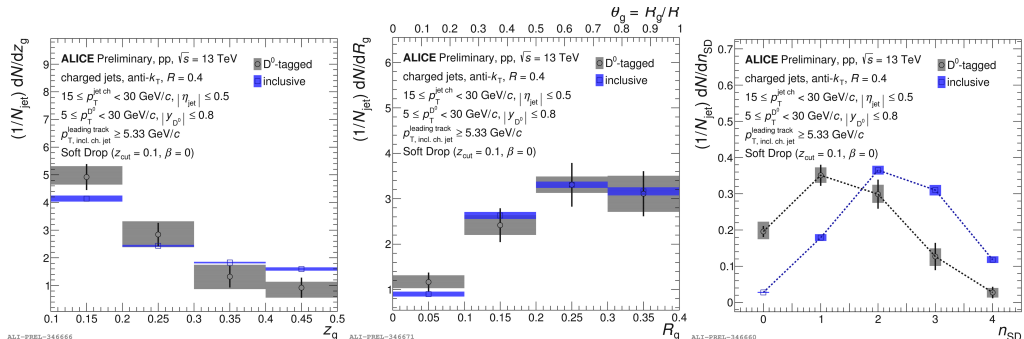


Fig. 2. Substructure variables z_g (left), θ_g (center) and n_{SD} (right) of D^0 -tagged charged-particle jets compared to inclusive charged-particle jets, in pp collisions at $\sqrt{s} = 13$ TeV.

the later evolution of the jets. Identification of jets initiated by heavy-flavor quarks therefore allow for direct access to jets initiated by quark fragmentation. Jet fragmentation is flavor dependent due to the color charge of the initial parton and also due to quark-mass effects on the radiation pattern. In the LHC energy regime, most jets originate from gluon fragmentation and are typically softer and wider than quark jets due to their larger color charge [13]. Charged particles with a mass $m > 0$ and energy E emit radiation that is suppressed below angles $\theta \approx m/E$ with respect to the axis of the radiator. This so-called dead-cone effect is expected to be present in jets containing heavy flavor [14, 15]. As a consequence, heavy-flavor quarks fragment hard, meaning that on average, radiation by the heavy parton carries a smaller fraction of the momentum than in the case of light partons. The ALICE Collaboration recently reported the first direct observation of the QCD dead-cone by using iterative declustering techniques to reconstruct the parton shower of charm quarks [16].

The consequences of the dead-cone effect on heavy flavor jet fragmentation can be also seen in Fig. 2, which shows the first measurement of groomed jet substructure of D^0 -tagged jets, compared to that of inclusive jets, in pp collisions at $\sqrt{s} = 13$ TeV. While the slightly different trends in z_g and θ_g between charmed and inclusive jets give a hint about flavor-dependent jet substructure, on average, there is about one less hard soft-drop splitting in charm jets than in inclusive jets. This fact is consistent with harder heavy-flavor fragmentation caused by the massive quarks.

While the production of heavy-flavor mesons via fragmentation follows a common pattern in different systems, recent measurements show that this universality is broken in the baryonic sector [17, 18]. Although several theoretical scenarios are proposed, including enhanced color reconnection with color-string junctions, statistical hadronization with enhanced baryonic states as well as quark coalescence [19–21], the proper description of charmed-baryon production still remains a challenge. The reconstruction of heavy-flavor hadrons within a jet allows for direct access to the fragmenta-

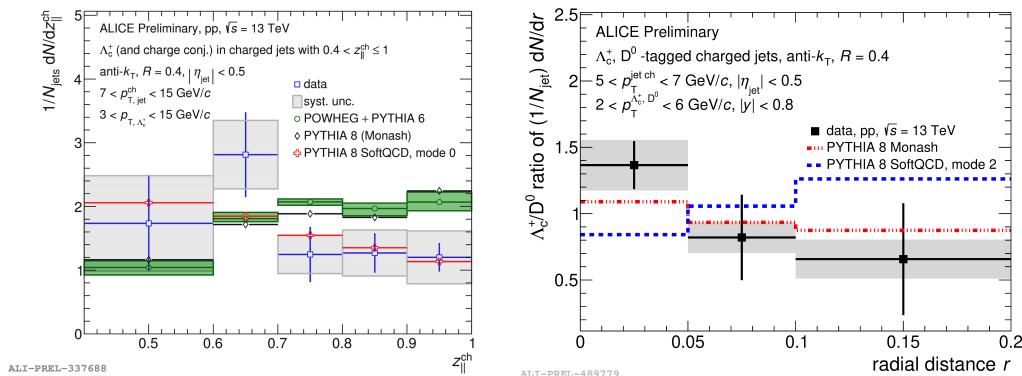


Fig. 3. Parallel momentum fraction $z_{||}$ of charged-particle jets tagged with Λ_c^+ baryons (left), and the Λ_c^+/D^0 ratio in function of angular distances (right). Both are compared to PYTHIA8 with the Monash tune [11] as well as the enhanced color-reconnection scenario [19].

tion of charm or beauty quark without the need to reconstruct the groomed jet substructure. ALICE measures both the parallel momentum fraction $z_{||}$ carried by the heavy-flavor hadron from the jet, and the radial angular distance of the heavy-flavor hadron from the jet axis for both the charmed D^0 mesons and the Λ_c^+ baryons. Figure 3 shows $z_{||}$ distribution for jets with Λ_c^+ , as well as the Λ_c^+/D^0 ratio, compared to models.

While the $z_{||}$ shows similar longitudinal behavior to the case of D^0 mesons [7], the radial-distance dependent ratios suggest that on the average, the Λ_c^+ fragments closer to the jet axis than the D^0 . Interestingly, neither of the trends are reproduced by models assuming enhanced color reconnection with color-string junctions [19].

4. Jet substructure in heavy-ion collisions

In collisions of ultrarelativistic heavy-ions, jet substructure measurements access the modification of jet fragmentation by the deconfined medium. Figure 4 shows the fully unfolded groomed momentum fraction z_g and the groomed radius θ_g of $R = 0.2$ jets in Pb–Pb compared to pp collisions at $\sqrt{s_{\text{NN}}} = 5.02$ TeV, as well as their ratios compared to several model calculations. The combinatorial background is suppressed using event-wise constituent subtraction, and a strong grooming condition of $z_{\text{cut}} = 0.2$ is applied. The distributions in z_g , representing the structure parallel to the jet axis, show no modification within uncertainties, The transverse quantity θ_g , however, displays a suppression of large angles, and an enhancement of small angles, hinting that the medium filters out wider subjets. Models with incoherent energy loss as well as fully coherent energy loss with gluon filtering qualitatively describe the data (see Ref. [22] and references therein).

Another way to access the details of radiation patterns is to construct observables that probe subjets (or more closely collimated prongs of particles)

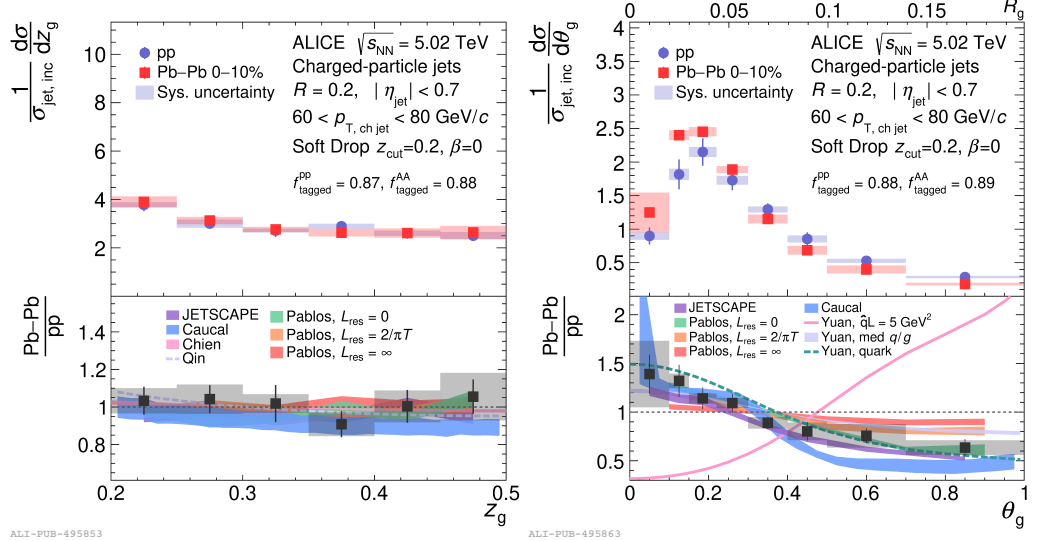


Fig. 4. Unfolded z_g (left) and θ_g distributions (right) for charged-particle jets in pp collisions compared to those in Pb–Pb collisions at $\sqrt{s_{\text{NN}}} = 5.02$ TeV with $z_{\text{cut}} = 0.2$ for 0–10% centrality and $R = 0.2$, in the $60 < p_{\text{T, ch jet}} < 80$ GeV/ c jet transverse-momentum range [22].

within a jet. One such class of variables is N -subjettiness [23], defined as

$$\tau_N = \frac{1}{p_{\text{T}}^{\text{jet}} R} \sum_k p_{\text{T},k} \min(\Delta R_{1,k}, \Delta R_{2,k}, \dots, \Delta R_{N,k}), \quad (3)$$

where k runs over the constituents of the jet, and $\Delta R_{i,k}$ are the distances of each subjet candidate $1 \leq i \leq N$ and the constituent k . By construction $\tau_N \approx 1$ in case the number of subjet prongs is less than N , and $\tau_N \approx 0$ otherwise. The distribution of τ_2/τ_1 will therefore be sensitive to the occurrence of 2-pronged vs. 1-pronged jets. Subjet fragmentation can also be accessed by reclustering jets using a smaller resolution parameter, $r < R$, and then characterize leading subjets with momentum fraction

$$z_r = \frac{p^{\text{leading subjet}}}{p^{\text{jet}}}. \quad (4)$$

Figure 5 (left) shows the first measurement of τ_2/τ_1 distributions, in Pb–Pb collisions at $\sqrt{s_{\text{NN}}} = 2.76$ TeV, with C/A reclustering and SD grooming [24]. The data show no significant modification within the current precision compared to PYTHIA6 and 8 simulations [11, 25]. In Figure 5 (right), the subjet fragmentation z_r is shown in Pb–Pb collisions at $\sqrt{s_{\text{NN}}} = 5.02$ TeV and a subjet resolution parameter $r = 0.1$. Consistently with model predictions, the data show hints of medium modification in the quark-dominated range around $z_r \approx 1$.

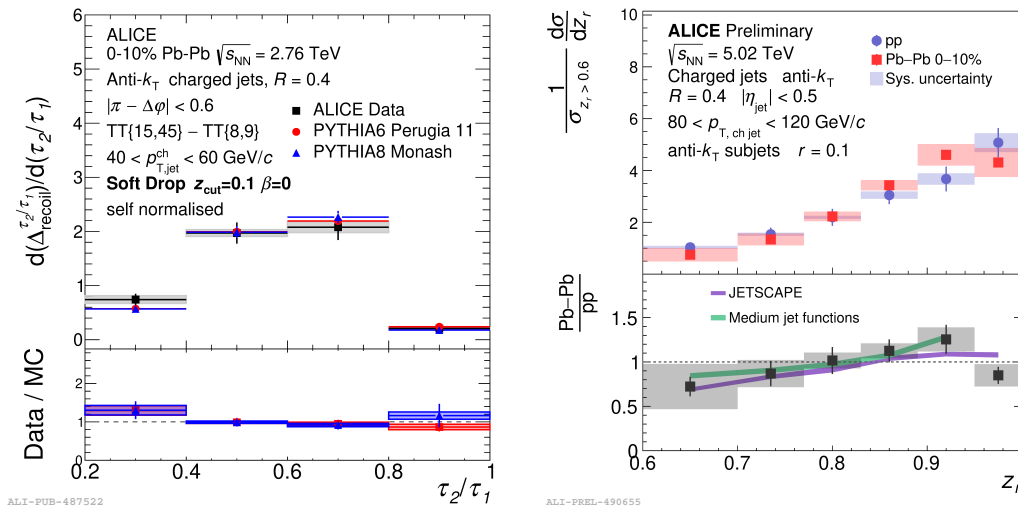


Fig. 5. Left: fully corrected τ_2/τ_1 distributions with SD grooming in Pb–Pb collisions at $\sqrt{s_{\text{NN}}} = 2.76$ TeV for charged-hadron jets with $R = 0.4$ in the $40 < p_{\text{T, ch jet}} < 60$ GeV/ c range, compared to models [24]. Right: Subjet fragmentation z_r in Pb–Pb collisions at $\sqrt{s_{\text{NN}}} = 5.02$ TeV in $80 < p_{\text{T, ch jet}} < 120$ GeV/ c range, compared to models.

This contribution summarized some of the recent results on jet substructure observables from the ALICE Collaboration. Measurements in pp collisions primarily serve to test predictions of pQCD calculations and hadronization models. Hard pQCD processes can be separated from soft radiation using grooming techniques. Flavor-dependent jet substructure measurements can be used to explore heavy-flavor fragmentation and help in disentangling color-charge and mass effects. Groomed jet substructures provide possibility to explore flavor and mass-dependent fragmentation. ALICE presented the first direct observation of the dead cone in hadronic collisions and demonstrated harder heavy-flavor fragmentation in groomed D^0 -tagged jets. Jet substructure measurements in Pb–Pb collisions aim for the understanding of jet modification by the hot and dense deconfined medium.

The upcoming LHC Run–3 data-taking phase with higher luminosity [26] will allow for precision measurements of beauty-jet substructure as well as detailed measurements in the charm baryonic sector. These will allow for the separation of color-charge and mass effects as well as the understanding of fragmentation in details. Future heavy-ion measurements can explore the details of jet–medium interaction, further facilitating model development and moving toward a deeper understanding of the non-perturbative domain of the strong interaction.

This work has been supported by the Hungarian NKFIH/OTKA FK 131979 and K 135515 grants, as well as the NKFIH 2019-2.1.6-NEMZ_KI-2019-00011 project.

REFERENCES

1. *Abelev B.B. et al.* [ALICE Collaboration] Performance of the ALICE Experiment at the CERN LHC // *Int. J. Mod. Phys. A.* — 2014. — V. 29. — P. 1430044. — arXiv:1402.4476 [nucl-ex].
2. *Cacciari M., Salam G.P., Soyez G.* The anti- k_t jet clustering algorithm // *JHEP.* — 2008. — V. 04. — P. 063. — arXiv:0802.1189 [hep-ph].
3. *Cunqueiro L., Płoskoń M.* Searching for the dead cone effects with iterative declustering of heavy-flavor jets // *Phys. Rev. D.* — 2019. — V. 99, no. 7. — P. 074027. — arXiv:1812.00102.
4. *Larkoski A.J., Marzani S., Soyez G., Thaler J.* Soft Drop // *JHEP.* — 2014. — V. 05. — P. 146. — arXiv:1402.2657 [hep-ph].
5. *Dokshitzer Y.L., Leder G.D., Moretti S., Webber B.R.* Better jet clustering algorithms // *JHEP.* — 1997. — V. 08. — P. 001. — arXiv:hep-ph/9707323.
6. *Acharya S. et al.* [ALICE Collaboration] Exploration of jet substructure using iterative declustering in pp and Pb–Pb collisions at LHC energies // *Phys. Lett. B.* — 2020. — V. 802. — P. 135227. — arXiv:1905.02512.
7. *Vértési R. et al.* [ALICE Collaboration] Jet measurements with ALICE: substructure, dead cone, charm jets // *PoSL.* — 2021. — V. HCP2020. — P. 143. — arXiv:2009.11228.
8. *Larkoski A.J., Thaler J., Waalewijn W.J.* Gaining (Mutual) Information about Quark/Gluon Discrimination // *JHEP.* — 2014. — V. 11. — P. 129. — arXiv:1408.3122 [hep-ph].
9. *Acharya S. et al.* [ALICE Collaboration] Measurements of the groomed and ungroomed jet angularities in pp collisions at $\sqrt{s} = 5.02$ TeV. — 2021. — 7. — arXiv:2107.11303.
10. *Almeida L.G., Ellis S.D., Lee C., Sterman G., Sung I., Walsh J.R.* Comparing and counting logs in direct and effective methods of QCD resummation // *JHEP.* — 2014. — V. 04. — P. 174. — arXiv:1401.4460 [hep-ph].
11. *Sjostrand T., Mrenna S., Skands P.Z.* A Brief Introduction to PYTHIA 8.1 // *Comput. Phys. Commun.* — 2008. — V. 178. — P. 852–867. — arXiv:0710.3820 [hep-ph].
12. *Bellm J., others.* Herwig 7.0/Herwig++ 3.0 release note // *Eur. Phys. J. C.* — 2016. — V. 76, no. 4. — P. 196. — arXiv:1512.01178.
13. *Kluth S.* Tests of Quantum Chromo Dynamics at e+ e- Colliders // *Rept. Prog. Phys.* — 2006. — V. 69. — P. 1771–1846. — arXiv:hep-ex/0603011.

14. *Dokshitzer Y.L., Khoze V.A., Troian S.I.* On specific QCD properties of heavy quark fragmentation ('dead cone') // J. Phys. G. — 1991. — V. 17. — P. 1602–1604.
15. *Thomas R., Kampfer B., Soff G.* Gluon emission of heavy quarks: Dead cone effect // Acta Phys. Hung. A. — 2005. — V. 22. — P. 83–91. — arXiv:hep-ph/0405189.
16. *Acharya S. et al.* [ALICE Collaboration] Direct observation of the dead-cone effect in QCD. — 2021. — 6. — arXiv:2106.05713.
17. *Acharya S. et al.* [ALICE Collaboration] Λ_c^+ production and baryon-to-meson ratios in pp and p-Pb collisions at $\sqrt{s_{NN}} = 5.02$ TeV at the LHC. — 2020. — 11. — arXiv:2011.06078.
18. *Acharya S. et al.* [ALICE Collaboration] Measurement of the cross sections of Ξ_c^0 and Ξ_c^+ baryons and branching-fraction ratio $\text{BR}(\Xi_c^0 \rightarrow \Xi^- e^+ \nu_e) / \text{BR}(\Xi_c^0 \rightarrow \Xi^- \pi^+)$ in pp collisions at 13 TeV. — 2021. — 5. — arXiv:2105.05187.
19. *Christiansen J.R., Skands P.Z.* String Formation Beyond Leading Colour // JHEP. — 2015. — V. 08. — P. 003. — arXiv:1505.01681.
20. *He M., Rapp R.* Charm-Baryon Production in Proton-Proton Collisions // Phys. Lett. B. — 2019. — V. 795. — P. 117–121. — arXiv:1902.08889.
21. *Plumari S., Minissale V., Das S.K., Coci G., Greco V.* Charmed Hadrons from Coalescence plus Fragmentation in relativistic nucleus-nucleus collisions at RHIC and LHC // Eur. Phys. J. C. — 2018. — V. 78, no. 4. — P. 348. — arXiv:1712.00730.
22. *Acharya S. et al.* [ALICE Collaboration] Measurement of the groomed jet radius and momentum splitting fraction in pp and Pb–Pb collisions at $\sqrt{s_{NN}} = 5.02$ TeV. — 2021. — 7. — arXiv:2107.12984.
23. *Thaler J., Van Tilburg K.* Identifying Boosted Objects with N-subjettiness // JHEP. — 2011. — V. 03. — P. 015. — arXiv:1011.2268 [hep-ph].
24. *Acharya S. et al.* [ALICE Collaboration] First measurements of N-subjettiness in central Pb–Pb collisions at $\sqrt{s_{NN}} = 2.76$ TeV. — 2021. — 5. — arXiv:2105.04936.
25. *Sjostrand T., Mrenna S., Skands P.Z.* PYTHIA 6.4 Physics and Manual // JHEP. — 2006. — V. 05. — P. 026. — arXiv:hep-ph/0603175.
26. *Noferini F. et al.* [ALICE Collaboration] ALICE results from Run-1 and Run-2 and perspectives for Run-3 and Run-4 // J. Phys. Conf. Ser. — 2018. — V. 1014, no. 1. — P. 012010.